JACS
JOURNAL OF THE AMERICAN CHEMICAL SOCIETY
Article
pubs.acs.org/JACS

Single-Molecule Conductance in Atomically Precise Germanium Wires

Timothy A. Su,[†,§] Haixing Li,[‡,§] Vivian Zhang,[†] Madhav Neupane,[†] Arunabh Batra,[‡] Rebekka S. Klausen,[†,⊥] Bharat Kumar,[†,∥] Michael L. Steigerwald,*[,†] Latha Venkataraman,*[,†,‡] and Colin Nuckolls*[,†]

[†]Department of Chemistry, Columbia University, New York, New York 10027, United States
[‡]Department of Applied Physics and Applied Mathematics, Columbia University, New York, New York 10027, United States

Supporting Information

ABSTRACT: While the electrical conductivity of bulk-scale group 14 materials such as diamond carbon, silicon, and germanium is well understood, there is a gap in knowledge regarding the conductivity of these materials at the nano and molecular scales. Filling this gap is important because integrated circuits have shrunk so far that their active regions, which rely so heavily on silicon and germanium, begin to resemble ornate molecules rather than extended solids. Here we unveil a new approach for synthesizing atomically discrete wires of germanium and present the first conductance measurements of molecular germanium using a scanning tunneling microscope-based break-junction (STM-BJ) technique. Our findings show that germanium and silicon wires are nearly identical in conductivity at the molecular scale, and that both are much more conductive than aliphatic carbon. We demonstrate that the strong donor ability of C−Ge σ-bonds can be used to raise the energy of the anchor lone pair and increase conductance. Furthermore, the oligogermane wires behave as conductance switches that function through stereoelectronic logic. These devices can be trained to operate with a higher switching factor by repeatedly compressing and elongating the molecular junction.

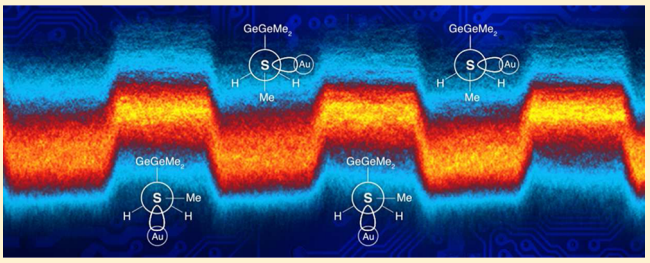

INTRODUCTION

Here we describe both the first deterministic synthesis of long, linear permethyloligogermanes and the first single-molecule conductance measurements on these atomically precise strands of germanium (Figure 1). An understanding of charge transport in atomically precise, molecular-scale germanium will inform the transport issues and opportunities in ever-smaller silicon−germanium integrated circuits.[1] Moreover, nanoscale forms of germanium such as germanene,[2,3] germanium quantum dots,[4] and germanium nanowires[5−9] are emerging as new materials with interesting electronic properties.

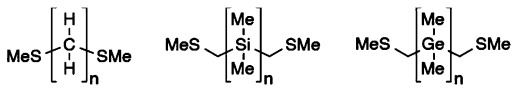

C*n* *(n=4-8)* **Si*n*** *(n=1-10)* **Ge*n*** *(n=1-10)*

The synthesis that is developed here allows us to easily functionalize these germanium wires with aurophilic methylthiomethyl groups on their termini to allow connection to gold electrodes. Using the scanning tunneling microscope-based break-junction (STM-BJ) method, we find that each **Ge*n*** oligomer is more conductive than its **Si*n*** isostructure due to the enhanced interaction in the contact group between the sulfur lone pair and the more strongly donating C−Ge σ-bond. However, adding an additional Ge−Ge σ-bond in the germanium wires has essentially the same effect on the magnitude of conductance as adding an additional Si−Si σ-bond in silicon wires. The Au−**Ge*n***−Au junction switches to a high-conductance (G) state only when both terminal Me−S−CH_2−$GeMe_2$− dihedral angles are twisted into *ortho* configurations, suggesting a possible route to an "AND" logic gate that operates by means of a stereoelectronic effect. Furthermore, we find that the repeated compression−elongation of the Au−**Ge*n***−Au junction causes the device to switch with a higher conductance magnitude with each successive cycle; these cycles effectively mold the electrodes into an optimal morphology for mechanically manipulating the geometry of the molecule in the junction.

RESULTS AND DISCUSSION

Synthesis. In order to study the conductance properties of molecular germanium, we needed to develop a new synthesis that was robust and produced linear-chain oligogermane wires in a stepwise fashion. Though germanium oligomers have been known since 1925,[10] methods for the facile synthesis and isolation of long (n > 6) linear oligogermanes have not been

Received: August 3, 2015

DOI: 10.1021/jacs.5b08155
J. Am. Chem. Soc. XXXX, XXX, XXX−XXX

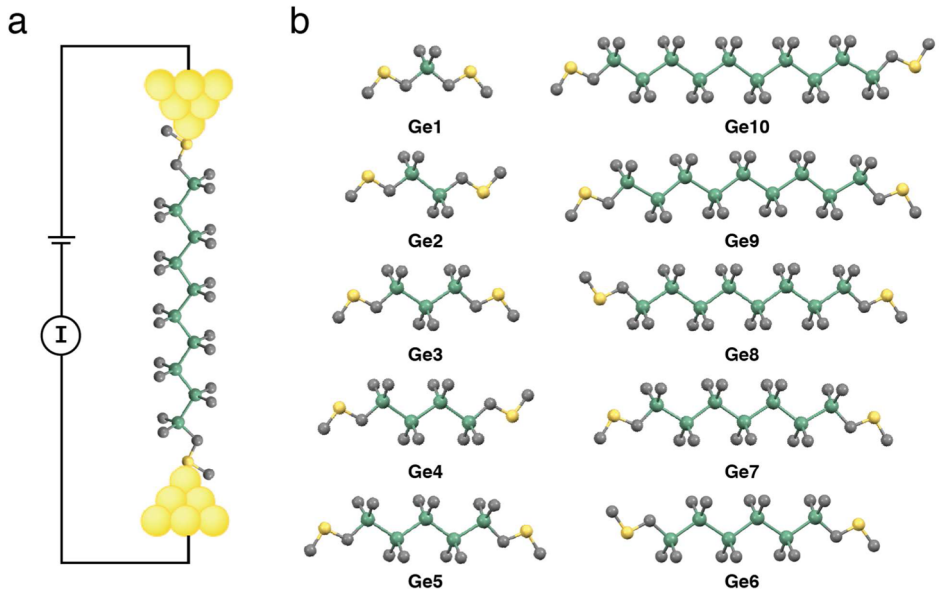

Figure 1. (a) STM-BJ experimental diagram of Au−**Ge10**−Au junction. (b) DFT-optimized structures for the **Ge1**−**Ge10** series with backbone dihedrals held at 180°. Ge, green; C, gray; S, yellow; H omitted for clarity.

reported.[11−15] Wurtz coupling between Me_3GeCl and Me_2GeCl_2 has been used to synthesize long oligogermanes ($\leq Ge_{10}Me_{22}$), but these reactions give low-yielding mixtures that are difficult to separate and products that are not functionalized.[16]

Here we introduce a new method for synthesizing an entire series of permethyloligogermanes (from n = 1−10) that are terminated with methylthiomethyl contacts in high yields with easy purification. Our approach was inspired by the iterative synthesis of α,ω-diphenylpermethyloligogermanes (Ph-$[GeMe_2]_n$-Ph) for n = 1−5 pioneered by Kumada and co-workers.[17] They observed low yields for this reaction due to the tendency of Ge−Ge bonds to disproportionate in the presence of strong nucleophiles such as dimethylphenylgermyl lithium. We were able to prevent oligogermane disproportionation by attenuating the strength of the nucleophile via transmetalation with $MgBr_2$, thereby accessing high yields (62−87%) of the longer oligomers. This simple adaptation has enabled us to achieve the first deterministic synthesis of germanium oligomers with n > 6. Using this new approach we have synthesized the longest linear oligogermane ($Ge_{11}Me_{22}Ph_2$) reported to date (see Supporting Information (SI) for details).

Scheme 1 illustrates our iterative approach to synthesizing the $[GeMe_2]_n$ oligogermanes (n = 1−10) terminated by electrode-binding methylthiomethyl end groups (**Ge1**−**Ge10**, Figure 1). We reduce chlorodimethylphenylgermane with lithium metal[17] and then transmetalate with $MgBr_2$ to access dimethylphenylgermyl magnesium bromide **1**. We grow α,ω-diphenyloligogermane **2** outward, two germanium subunits at a time, by treating α,ω-dichlorooligogermane **3** with 2 equiv of **1**. After purification of **2**, protiodegermylation of α,ω-diphenyloligogermane **2** under acidic conditions furnishes the chain-extended α,ω-dichlorooligogermane **3**.[18] We functionalize α,ω-dichlorooligogermane **3** with electrode contacts (CH_2SMe) by reacting **3** with methylthiomethyl lithium[19] to furnish the final α,ω-bis(methylthiomethyl)oligogermanes **Ge1**−**Ge10**.

Conductance Measurements. We measured the single-molecule conductance of oligogermanes **Ge1**−**Ge10** with the STM-BJ technique.[20] In brief, Au−**Ge***n*−Au junctions are

Scheme 1. Iterative Synthesis of Permethyloligogermanes Terminated with Methylthiomethyl End Groups[a]

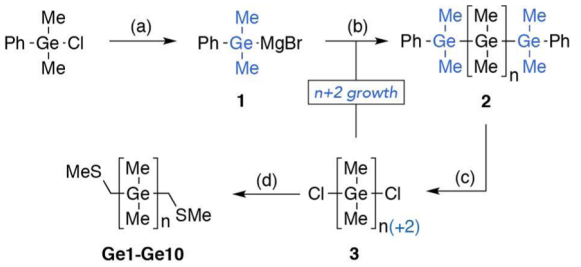

[a]The n+2 oligomer growth cycle is depicted in blue. Reagents and conditions: (a) *i.* Li, THF; *ii.* $MgBr_2$, THF. (b) THF, 0 °C; for n = 3−10, yields are 62−87%. (c) *i.* CF_3SO_3H, CH_2Cl_2; *ii.* $Et_3N{\cdot}HCl$, Et_2O; for n = 3−10, yields are 65−94%. (d) *n*-BuLi, TMEDA, CH_3SCH_3, THF; for n = 1−10, yields are 40−84%.

formed by repeatedly breaking and forming point contacts between Au tip and substrate electrodes in a dilute (0.10−1.00 mM) solution of the oligogermane in 1,2,4-trichlorobenzene under ambient conditions. After the Au−Au point contact is broken, the aurophilic thiomethyl groups[21] on the oligogermane bind the electrodes to form a Au−**Ge***n*−Au junction. Conductance is measured across the gap as a function of tip−substrate displacement, and the resulting traces reveal molecule-dependent plateaus signifying junction formation with conductance values below G_0 ($2e^2/h$), the quantum of conductance describing a single Au−Au atomic contact.[22] The junction breaks once the distance between the electrodes becomes too large for the molecule to bridge this gap. We form and break thousands of molecular junctions and analyze all measured traces using logarithm-binned one-dimensional (1D) and two-dimensional (2D) histograms. 1D histograms provide a distribution of all measured conductance values from all traces; 2D histograms sum all conductance values while retaining relative displacement information.[23]

The 1D histograms for the conductance measurements of **Ge1**−**Ge10** are shown in Figure 2a. The peak positions demonstrate a clear exponential decrease in conductance as the

DOI: 10.1021/jacs.5b08155
J. Am. Chem. Soc. XXXX, XXX, XXX−XXX

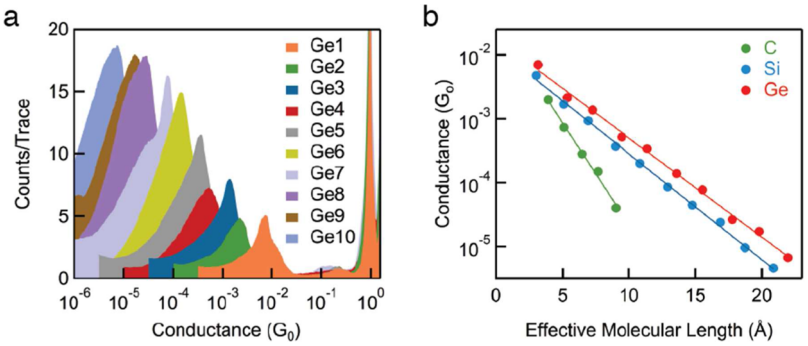

Figure 2. (a) Logarithm-binned 1D conductance histograms of **Ge1**−**Ge10**, each comprising thousands of measurement traces. (b) Conductance peak positions from the simple elongation measurements of **C4**−**C8**, **Si1**−**Si10**, and **Ge1**−**Ge10** (panel a) plotted against effective molecular length (L, in Å) give the decay constant β. β_C = 0.74 ± 0.03 Å^{-1}, β_{Si} = 0.39 ± 0.01 Å^{-1}, and β_{Ge} = 0.36 ± 0.01 Å^{-1}.

molecular length increases from n = 1−10. We obtain β for the **Ge***n* series in Figure 2b by plotting the conductance peaks from Figure 2a against the effective molecular length (L) on a semilog plot and fitting a line through these points, with $G = R^{-1} e^{-\beta L}$. For every molecule described here, L is defined as the distance between the two distal methylene carbons in the density functional theory (DFT)-optimized structures, R is an effective contact resistance, and β is the conductance decay parameter. β describes the extent to which conductance in a given oligomeric material decreases as the number of repeat units increases, and depends strongly on the extent by electronic delocalization (conjugation) in the backbone. We find that conductances from **Ge1**−**Ge10** follow an exponential in L with β_{Ge} = 0.36 ± 0.01 Å^{-1} (0.74 ± 0.02 n^{-1}). This signifies that charge transport in molecular germanium (up to **Ge10**) occurs through a coherent tunneling mechanism.[24] Figure S1 plots the conductances of all molecules against n.

We find that the decay constant of oligogermanes is very similar to that of oligosilanes (β_{Si} = 0.39 ± 0.01 Å^{-1}, 0.75 ± 0.01 n^{-1}) and oligo-*p*-phenylenes[25] but much shallower than that of alkanes (β_C = 0.74 ± 0.03 Å^{-1}, 0.94 ± 0.05 n^{-1}). Our experimental findings are consistent with calculations of Matsuura on permethylated n = 2−6 oligomers of carbon, silicon, and germanium with −CH_2SH linker end groups.[26] Matsuura calculated β_C = 0.71 Å^{-1} for alkanes, β_{Si} = 0.31 Å^{-1} for oligosilanes, and β_{Ge} = 0.34 Å^{-1} for oligogermanes. The β values determined from these computations are remarkably close to what we observe experimentally.

Because the repeat units in the alkane, silane, and germane oligomers are single atomic units, β can serve as an index for comparing the intrinsic electrical σ-conductivity of the group 14 elements at the single-bond level. The near-identical β values for silanes and germanes suggest that Si−Si and Ge−Ge σ-bonds are similar in charge transport ability at the molecular scale, and that both are much more conductive than C−C σ-bonds. This is perhaps not surprising based on the relationship between conductance and conjugation or through the molecule.[27] Alkanes demonstrate a high β value because of the weak delocalization in the C−C σ-backbone.[28] We previously established that the shallow β value[29,30] observed for oligosilanes is related to the strong conjugation in the Si−Si bonds, which are much larger and more strongly interacting compared to C−C σ-bond orbitals.[31−35] Since oligosilanes and oligogermanes are known to display similar degrees of σ-conjugation based on the spectroscopic and electrochemical studies of group 14 oligomers from the past several decades, it is not surprising that they also show near-identical β values here. Drenth and co-workers characterized the ultraviolet absorption in a series of peralkylated silicon and germanium oligomers (n = 2−6).[36] By measuring the transition energy as a function of n, they elucidated the resonance stabilization energy between adjacent atoms and ultimately demonstrated that silane and germane oligomers share the same strength of conjugation between their σ-bonding orbitals. Boberski et al. and Okano et al. studied σ-conjugation by probing the electrochemical oxidation potentials of permethylated silicon and germanium oligomers.[37,38] The data from these two studies demonstrated that the first oxidation potential decreased by roughly the same extent in silanes and germanes with increasing n. We find the same to be true for the molecules studied here (Figure S1). Importantly, these single-molecule measurements demonstrate that the numerous studies devoted to understanding the nature of orbital interactions can serve as a predictive tool for designing molecular electronic components.

Though the **Ge***n* and **Si***n* series are near-identical in β value, the conductance of each germanium oligomer is ∼1.5 times higher than that of its silicon counterpart; this difference in conductance arises from subtle differences in the way H_2C−$GeMe_2$ and H_2C−$SiMe_2$ σ-bonds interact with the S pπ lone pair at each termini. C−Ge σ-bonds are more electron donating than C−Si σ-bonds because they are higher in energy and more diffuse.[39−44] The molecular orbital most relevant to conductance in these systems is the HOMO, which features strong S lone pair orbital character.[30,45−48] The destabilizing interaction between the filled S lone pair and the more strongly donating C−Ge σ-bond raises the HOMO energy closer toward the Au Fermi level, thereby increasing conductance.[45,47,49]

This line of reasoning is consistent with our DFT calculations of **Si1** and **Ge1** (see SI for computational details). **Ge1** (−5.49 eV) possesses a higher HOMO energy than **Si1** (−5.56 eV) in conformations where the S lone pair and C−Si(Ge) σ-bond are coplanar. Our calculations are supported by Glass et al., who demonstrated that the ionization energy of organosulfides is inversely proportional to the donor ability of the σ-bond in the β-position relative to the S atom.[50] We also find evidence for these destabilizing effects in our estimations of the HOMO energy from cyclic voltammetry studies on the **Si***n* and **Ge***n* series (Figure S1). As n increases, the HOMO energies in both **Ge***n* and **Si***n* rise with a similar slope but are offset by a roughly constant energy value. These results demonstrate that we can utilize the differential donor ability of σ-bonds to tune the energetics of the linker lone pair, and therefore, conductance.

DOI: 10.1021/jacs.5b08155
J. Am. Chem. Soc. XXXX, XXX, XXX−XXX

We also note that there is an appreciable odd−even effect on conductance that exists for the **Ge***n* series in Figure 2b, where the even-numbered oligomers fall below the decay line (error is within the size of the marker). The odd−even effect is also manifested in the peak shapes of the odd and even oligomers—the odd oligomers are much sharper in conductance width than the even ones (Figures S3 and S4). This alternant trend seems to occur in the **Si***n* series as well, although with a smaller magnitude. These odd−even effects may stem from the strong vicinal hyperconjugation in germanes, and are the subject of further study.[51]

Stereoelectronic Switching. 2D histogram analysis (Figure S5) and tunnel coupling calculations (Figure S6, details in SI) suggest that each **Ge***n* oligomer acts as a mechanically triggered switch that operates with a stereoelectronic mechanism analogous to what was previously described for **Si1**−**Si10**.[30] In brief, elongating the Au−**Ge***n*−Au junction changes the lowest energy configuration of the two terminal Me−S−CH_2−$GeMe_2$− dihedrals from the sterically favored *anti* (A) conformation to the mechanically favored *ortho* (O) conformation (Figure 3). The conductance-switching

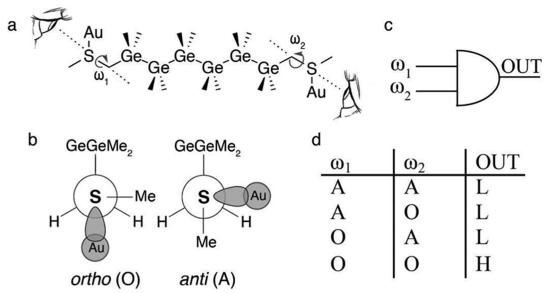

Figure 3. (a) Molecular structure of $\mathbf{Ge_6}$ with two terminal Me−S−CH_2−$GeMe_2$− dihedrals ω_1 and ω_2. (b) Newman projections of the mechanically favored *ortho* (left) and sterically favored *anti* (right) dihedral configurations. (c) Standard representation of an AND logic gate with ω_1 and ω_2 as inputs for stereoelectronic switching. (d) Truth table for observing either the low-conducting (L) or high-conducting (H) state based on tunnel coupling calculations.

event likely embodies a shift in molecular geometry from the low-conducting A-A and O-A configurations to the high-conducting O-O configuration. The conjugation in the **Ge***n* σ-backbone should enable this mechanism of switching because it electronically couples the two terminal Me−S−CH_2−$GeMe_2$− dihedrals.

George et al. modeled the relationship between conformation and conductance in hydrogenated oligosilanes and found that conductance (and σ-conjugation) is maximized when the Si−Si−Si−Si dihedrals have an *anti* (ω = 180°) geometry.[52] Michl and co-workers[53,54] demonstrated that permethyloligosilanes settle into *transoid* (ω = 160−175°)[55] rather than *anti* minimum energy geometries due to steric effects from the methyl groups.[56] In our previous calculations on the Au−**Si4**−Au system, we found that the internal Si−Si−Si−Si backbone geometry maintains a relatively constant dihedral angle that averages around ω = 168°. Here we find that the Ge−Ge−Ge−Ge dihedral in the Au−**Ge4**−Au system remains relatively constant with an average of ω = 172° (Table S4). We hypothesize that the tetragermane dihedral is closer to *anti* than the tetrasilane because the Ge−Ge bonds (2.51 Å) are longer than the Si−Si bonds (2.38 Å), which would reduce the steric repulsion from the methyl groups. These results suggest that the σ-conjugation in the oligogermane backbone is slightly stronger than in the oligosilane backbone, since the dihedral angles are closer to *anti*. This would account for the lower β value that we observe experimentally for the **Ge***n* series and the higher tunnel coupling ratio that we calculate for the high- and low-*G* states in oligogermanes versus oligosilanes (Figure S6). Following this line of reasoning, we predict that structurally constraining the σ-backbone to ω = 180° in group 14 wires may enable even lower β values and higher switching factors to be observed. Tamao and co-workers have synthesized such conformationally locked oligosilanes and have demonstrated increased σ-conjugation in the context of charge transfer[57] and absorption[58] studies.

Our tunnel coupling calculations also demonstrate that, in principle, the **Ge***n* switches are capable of behaving as AND logic gates that follow the truth table in Figure 3, where the high-*G* state is only observed under the condition that both terminal dihedral angles are in the *ortho* state. We have not yet experimentally realized such a logic device because we can only indirectly set the dihedral configuration by regulating the inter-electrode distance; developing a precise method for controlling each dihedral input independently will enable the creation of a true stereoelectronic logic device.

Junction Training. In the simple elongation experiments described above, we continually widen the electrode gap until the molecular junction breaks. For all **Ge***n* oligomers, conductance switches from a low- to high-*G* state (Figure 4a) in the final ~2 Å of elongation with a factor that varies slightly from molecule to molecule (Figures S5 and S7). For instance, Au−**Ge5**−Au junctions demonstrate a switching factor

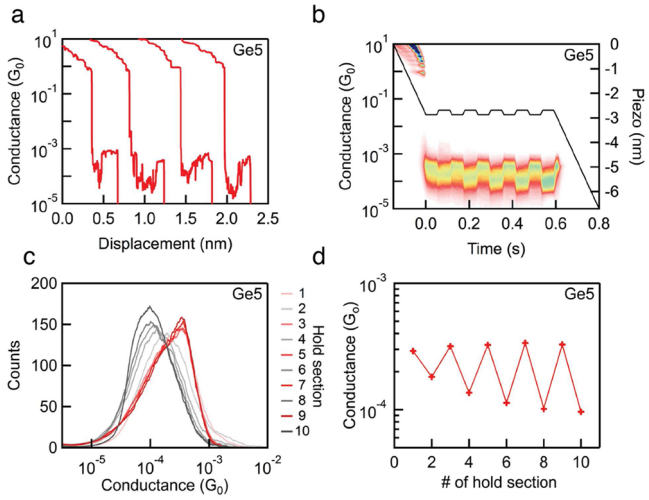

Figure 4. (a) Individual traces of **Ge5** demonstrate switching from low to high conductance as the molecular junction is elongated. (b) 2D histogram of five successive 2 Å compression−elongation cycles for the Au−$\mathbf{Ge_5}$−Au junction measured using a modified piezo ramp (black line). Switching is induced between low- and high-*G* states when the junction is pushed and pulled consecutively. The 2D histogram is constructed from all traces sustaining a junction over all ten hold sections. (c) 1D histograms compiled from each hold period after compressions (gray lines) and hold periods after elongations (red lines) from panel b. (d) The conductance peak positions from the 1D histograms in panel c plotted against the hold section. The ratio of conductance between the compression (low *G*) and elongation (high *G*) peaks gives the switching factor for a single cycle. The switching factors upon compression from cycles 1−5 are 1.6, 2.3, 2.9, 3.3, and 3.4, respectively.

DOI: 10.1021/jacs.5b08155
J. Am. Chem. Soc. XXXX, XXX, XXX−XXX

(defined as the ratio of the conductance of the high-*G* state to that of the low-*G* state) of 1.6 upon the initial elongation (Figure S7). Here we demonstrate that we can increase the switching factor beyond this initial ratio by repeatedly compressing and elongating the molecular junction with a modified piezo ramp (Figure 4b).

Instead of elongating the junction to rupture after we fully extend the Au−**Ge***n*−Au junction, we perform push−pull cycles by first compressing the electrode gap by 2 Å, holding the electrodes fixed for 50 ms, widening the electrode gap by 2 Å, then holding for 50 ms. Figure 4b shows a 2D histogram describing five consecutive push−pull cycles for the Au−**Ge5**−Au junction. Figure 4c compiles the conductance measured during each hold section into 1D histograms; the resulting conductance peak values are plotted in Figure 4d. Figure 4d shows that the first compression gives a switching factor of 1.6, and the final compression gives a switching factor of 3.4. Each successive push−pull cycle increases the switching factor and sharpness of switching, training the junction to perform increasingly better as a switch. We also find that the final switching factor for **Ge5** (3.4) is larger than for **Si6** (2.5) (Figure S8); this difference is likely related to the slightly stronger σ-conjugation in the germane backbone that we discussed in the subsection above.

The conductance trends in Figure 4 demonstrate that this junction training effect arises from the decreasing conductance of the low-*G* state. In each successive cycle, the elongation (high-*G*) conductance peak value remains constant whereas the compression (low-*G*) peak value decreases steadily (Figure 4d). Figure 4c reveals that in the first cycle, the compressed low-*G* state is broad in conductance and features a significant amount of high-*G* character. Every subsequent cycle narrows the conductance distribution by decreasing the amount of high-*G* character in the compressed low-*G* state; this in turn decreases the conductance of the low-*G* peak and maximizes the switching factor with each additional cycle.

As we described before, fully stretching the molecular junction imposes mechanical strain on the system.[30] The data here suggest that, for initial compression events, the system frequently relaxes by reorganizing the atomic electrode environment while sustaining the high-conducting O-O junction geometry. Repeatedly stretching and compressing the junction likely shapes the malleable electrodes into a structure where electrode surface reorganization is no longer the dominant relaxation pathway; instead, the system compensates for the changing interelectrode distance by twisting the junction's terminal dihedrals into a shorter, less conductive geometry. These cycles mechanically anneal[59] the electrodes into an optimal morphology for stereoelectronic switching and enable the junction to distinguish molecular conformations with more clarity.

Trouwborst et al. previously reported a similar junction training technique to create reproducible Au−Au point contacts from disordered electrode environments.[60] In that study, the authors organized the tip atoms by performing consecutive 1−2 Å compression−elongation cycles near the point of contact between two Au atoms at cryogenic temperatures, and in this way allowed the electrode atoms to probe different geometries and find the most stable configuration. It seems likely that we are organizing the electrodes here in much of the same way at room temperature, but are doing so with a molecular tether; this method might then serve as a valuable approach to organizing the atomic arrangement of the electrode surface in situations where direct contact between the electrodes is undesirable.

CONCLUSION

In this study we developed a new method for synthesizing long (>2 nm) molecular germanium wires with atomic precision that utilizes the attenuated nucleophilicity of germylmagnesium species. To demonstrate the utility of this system, we performed the first single-molecule conductance measurements on atomically defined molecular germanium wires. As in the silicon series, the germanium series behave as stereoelectronic switches activated by stretching or compressing our junction. Consecutive compression−elongation cycles train the molecular junction to both exhibit a higher switching factor and distinguish molecular geometries of disparate electronic character with more accuracy. Each **Ge***n* oligomer demonstrates a heightened conductance relative to its **Si***n* congener due to the stronger destabilizing interaction between the S lone pair and methylene−Ge σ-bond in the contact group. And yet, adding an extra Ge−Ge σ-bond to the **Ge***n* series has essentially the same effect on conductance magnitude as adding an extra Si−Si σ-bond to the **Si***n* series.

More broadly, these results show that Si and Ge molecular wires possess essentially the same length-dependent conductivity due to the similar extent of σ-conjugation in these systems. The intrinsic electrical conductivity of bulk silicon is the same order of magnitude as bulk germanium at room temperature, and both are many orders of magnitude more conductive than bulk diamond.[61] The periodic trends in molecular conductivity that we observe here therefore mirror group 14 conductivity trends in solid-state materials; this is not the case for stochastically grown Si and Ge nanowires where reported conductivities vary by many orders of magnitude due to a number of extrinsic factors.[6−9] We envision that the atomic precision in the molecular wires here will enable their use as reliable platforms for studying effects such as strain and doping in electronic materials, to not only probe the fundamental nature of these effects in bulk systems but also to inform the design of next-generation electronic circuit materials.

ASSOCIATED CONTENT

Supporting Information

The Supporting Information is available free of charge on the ACS Publications website at DOI: 10.1021/jacs.5b08155.

Supplemental figures, synthetic procedures, characterization of compounds, STM-BJ measurement details, and computational details (PDF)

AUTHOR INFORMATION

Corresponding Authors

*mls2064@columbia.edu
*lv2117@columbia.edu
*cn37@columbia.edu

Present Addresses

[⊥]R.S.K.: Department of Chemistry, The Johns Hopkins University, Baltimore, MD 21218, USA
[∥]B.K.: IBM Watson Research Center, Physical Sciences, 1101 Kitchawan Rd., Route 134, P.O. Box 218, Yorktown Heights, NY 10598, USA

Author Contributions

[§]T.A.S. and H.L. contributed equally to this work.

DOI: 10.1021/jacs.5b08155
J. Am. Chem. Soc. XXXX, XXX, XXX−XXX

Notes

The authors declare no competing financial interest.

■ ACKNOWLEDGMENTS

We thank James L. Leighton for insightful discussions and Brandon Fowler for mass spectrometry characterization. T.A.S. is supported by the NSF Graduate Research Fellowship under grant no. 11-44155. H.L. is supported by the Semiconductor Research Corporation and New York CAIST program. We thank the NSF for the support of these studies under grant no. CHE-1404922.

■ REFERENCES

(1) Markoff, J. IBM Discloses Working Version of a Much Higher-Capacity Chip. *New York Times* **2015** (July 9), B2.
(2) Ni, Z.; Liu, Q.; Tang, K.; Zheng, J.; Zhou, J.; Qin, R.; Gao, Z.; Yu, D.; Lu, J. *Nano Lett.* **2012**, *12*, 113.
(3) Bianco, E.; Butler, S.; Jiang, S.; Restrepo, O. D.; Windl, W.; Goldberger, J. E. *ACS Nano* **2013**, *7*, 4414.
(4) Heath, J. R.; Shiang, J. J.; Alivisatos, A. P. *J. Chem. Phys.* **1994**, *101*, 1607.
(5) Heath, J. R.; Legoues, F. K. *Chem. Phys. Lett.* **1993**, *208*, 263.
(6) Gu, G.; Burghard, M.; Kim, G. T.; Düsberg, G. S.; Chiu, P. W.; Krstic, V.; Roth, S.; Han, W. Q. *J. Appl. Phys.* **2001**, *90*, 5747.
(7) Mahenderkar, N. K.; Liu, Y.; Koza, J. A.; Switzer, J. A. *ACS Nano* **2014**, *8*, 9524.
(8) Barth, S.; Koleśnik, M. M.; Donegan, K.; Krstić, V.; Holmes, J. D. *Chem. Mater.* **2011**, *23*, 3335.
(9) Hanrath, T.; Korgel, B. A. *J. Phys. Chem. B* **2005**, *109*, 5518.
(10) Morgan, G. T.; Drew, H. D. K. *J. Chem. Soc., Trans.* **1925**, *127*, 1760.
(11) Amadoruge, M. L.; Weinert, C. S. *Chem. Rev.* **2008**, *108*, 4253.
(12) Weinert, C. S. *Dalt. Trans.* **2009**, 1691.
(13) Roewe, K. D.; Rheingold, A. L.; Weinert, C. S. *Chem. Commun.* **2013**, *49*, 8380.
(14) Wagner, H.; Baumgartner, J.; Müller, T.; Marschner, C. *J. Am. Chem. Soc.* **2009**, *131*, 5022.
(15) The hexagermane is the longest structurally characterized linear oligomer and was independently synthesized by Roewe et al. (ref 13) via Ge4Ph8 ring-opening and hydrogermolysis, as well as by Wagner et al. (ref 14) via germanium shuttling.
(16) Mochida, K.; Hata, R.; Chiba, H.; Seki, S.; Yoshida, Y.; Tagawa, S. *Chem. Lett.* **1998**, 263.
(17) Kumada, M.; Sakamoto, S.; Ishikawa, M. *J. Organomet. Chem.* **1969**, *17*, 235.
(18) Ruehl, K. E.; Matyjaszewski, K. *J. Organomet. Chem.* **1991**, *410*, 1.
(19) Peterson, D. J. *J. Org. Chem.* **1967**, *32*, 1717.
(20) Xu, B.; Tao, N. J. *Science* **2003**, *301*, 1221.
(21) Park, Y. S.; Whalley, A. C.; Kamenetska, M.; Steigerwald, M. L.; Hybertsen, M. S.; Nuckolls, C.; Venkataraman, L. *J. Am. Chem. Soc.* **2007**, *129*, 15768.
(22) Agraït, N.; Rodrigo, J.; Vieira, S. *Phys. Rev. B: Condens. Matter Mater. Phys.* **1993**, *47*, 12345.
(23) Kamenetska, M.; Koentopp, M.; Whalley, A.; Park, Y.; Steigerwald, M.; Nuckolls, C.; Hybertsen, M.; Venkataraman, L. *Phys. Rev. Lett.* **2009**, *102*, 126803.
(24) Salomon, A.; Cahen, D.; Lindsay, S.; Tomfohr, J.; Engelkes, V. B.; Frisbie, C. D. *Adv. Mater.* **2003**, *15*, 1881.
(25) Venkataraman, L.; Klare, J. E.; Nuckolls, C.; Hybertsen, M. S.; Steigerwald, M. L. *Nature* **2006**, *442*, 904.
(26) Matsuura, Y. *J. Appl. Phys.* **2014**, *115*, 043701.
(27) Venkataraman, L.; Klare, J. E.; Nuckolls, C.; Hybertsen, M. S.; Steigerwald, M. L. *Nature* **2006**, *442*, 904.
(28) Sandorfy, C. *Can. J. Chem.* **1955**, *33*, 1337.
(29) Klausen, R. S.; Widawsky, J. R.; Steigerwald, M. L.; Venkataraman, L.; Nuckolls, C. *J. Am. Chem. Soc.* **2012**, *134*, 4541.
(30) Su, T. A.; Li, H.; Steigerwald, M. L.; Venkataraman, L.; Nuckolls, C. *Nat. Chem.* **2015**, *7*, 215.
(31) Miller, R. D.; Michl, J. *Chem. Rev.* **1989**, *89*, 1359.
(32) Tsuji, H.; Terada, M.; Toshimitsu, A.; Tamao, K. *J. Am. Chem. Soc.* **2003**, *125*, 7486.
(33) Tamao, K.; Tsuji, H.; Terada, M.; Asahara, M.; Yamaguchi, S.; Toshimitsu, A. *Angew. Chem.* **2000**, *112*, 3425.
(34) Imhof, R.; Antic, D.; David, D. E.; Michl, J. *J. Phys. Chem. A* **1997**, *101*, 4579.
(35) Tsuji, H.; Michl, J.; Tamao, K. *J. Organomet. Chem.* **2003**, *685*, 9.
(36) Drenth, W.; Noltes, J. G.; Bulten, E. J.; Creemers, H. M. J. C. *J. Organomet. Chem.* **1969**, *17*, 173.
(37) Boberski, W. G.; Allred, A. L. *J. Organomet. Chem.* **1975**, *88*, 65.
(38) Okano, M.; Mochida, K. *Chem. Lett.* **1990**, 701.
(39) Wierschke, S. G.; Chandrasekhar, J.; Jorgensen, W. L. *J. Am. Chem. Soc.* **1985**, *107*, 1496.
(40) Lambert, J. B.; Zhao, Y.; Emblidge, R. W.; Salvador, L. a.; Liu, X.; So, J.-H.; Chelius, E. C. *Acc. Chem. Res.* **1999**, *32*, 183.
(41) Nguyen, K. A.; Gordon, M. S.; Wang, G. T.; Lambert, J. B. *Organometallics* **1991**, *10*, 2798.
(42) Lambert, J. B.; Wang, G. T.; Teramura, D. H. *J. Org. Chem.* **1988**, *53*, 5422.
(43) Eaborn, C.; Pande, K. C. *J. Chem. Soc.* **1960**, 1566.
(44) C−Ge bonds are better at stabilizing β-carbocation intermediates in the context of chemical reactivity for this very reason, accelerating reaction rates by 1−2 orders of magnitude relative to their organosilane congeners (refs 42 and 43).
(45) Klausen, R. S.; Widawsky, J. R.; Su, T. A.; Li, H.; Chen, Q.; Steigerwald, M. L.; Venkataraman, L.; Nuckolls, C. *Chem. Sci.* **2014**, *5*, 1561.
(46) Meisner, J. S.; Ahn, S.; Aradhya, S. V.; Krikorian, M.; Parameswaran, R.; Steigerwald, M.; Venkataraman, L.; Nuckolls, C. *J. Am. Chem. Soc.* **2012**, *134*, 20440.
(47) Engelkes, V. B.; Beebe, J. M.; Frisbie, C. D. *J. Am. Chem. Soc.* **2004**, *126*, 14287.
(48) Su, T. A.; Widawsky, J. R.; Li, H.; Klausen, R. S.; Leighton, J. L.; Steigerwald, M. L.; Venkataraman, L.; Nuckolls, C. *J. Am. Chem. Soc.* **2013**, *135*, 18331.
(49) Venkataraman, L.; Park, Y. S.; Whalley, A. C.; Nuckolls, C.; Hybertsen, M. S.; Steigerwald, M. L. *Nano Lett.* **2007**, *7*, 502.
(50) Glass, R. S.; Block, E.; Gruhn, N. E.; Jin, J.; Lorance, E.; Zakai, U. I.; Zhang, S. Z. *J. Org. Chem.* **2007**, *72*, 8290.
(51) Song, L.; Lin, Y.; Wu, W.; Zhang, Q.; Mo, Y. *J. Phys. Chem. A* **2005**, *109*, 2310.
(52) George, C. B.; Ratner, M. A.; Lambert, J. B. *J. Phys. Chem. A* **2009**, *113*, 3876.
(53) Piqueras, M. C.; Crespo, R.; Michl, J. *J. Phys. Chem. A* **2003**, *107*, 4661.
(54) Fogarty, H. A.; Imhof, R.; Michl, J. *Proc. Natl. Acad. Sci. U. S. A.* **2004**, *101*, 10517.
(55) Michl, J.; West, R. *Acc. Chem. Res.* **2000**, *33*, 821.
(56) We study permethylated oligosilanes and -germanes because they are much more stable than their hydrogenated structural analogues.
(57) Shibano, Y.; Sasaki, M.; Tsuji, H.; Araki, Y.; Ito, O.; Tamao, K. *J. Organomet. Chem.* **2007**, *692*, 356.
(58) Fukazawa, A.; Tsuji, H.; Tamao, K. *J. Am. Chem. Soc.* **2006**, *128*, 6800.
(59) Sabater, C.; Untiedt, C.; Palacios, J. J.; Caturla, M. J. *Phys. Rev. Lett.* **2012**, *108*, 205502.
(60) Trouwborst, M.; Huisman, E.; Bakker, F.; van der Molen, S.; van Wees, B. *Phys. Rev. Lett.* **2008**, *100*, 175502.
(61) Madelung, O. *Semiconductors: Data Handbook*, 3rd ed.; Springer: Berlin, 2004.

DOI: 10.1021/jacs.5b08155
J. Am. Chem. Soc. XXXX, XXX, XXX−XXX